

REPORTS

- by upward-propagating waves, leads to downward phase propagation of wind anomalies. The downward phase propagation creates what may be an illusion of downward influence, especially when the data are smoothed in time. Downward phase propagation does not in itself imply that anomalies at lower levels originate at upper levels. The stratosphere is modified by waves originating in the troposphere, altering the conditions for planetary-wave propagation in such a way as to draw mean-flow anomalies downward.
17. We used the National Centers for Environmental Prediction (NCEP) reanalysis data for 1000 to 10 hPa during 1958 to 2002 on a 2.5° longitude by 2.5° latitude grid. The NCEP reanalysis data were obtained from the National Oceanic and Atmospheric Administration—Cooperative Institute for Research in Environmental Sciences (NOAA-CIRES) Climate Diagnostics Center.
 18. For the Southern Hemisphere, we used NCEP data from 1979 to 2001. Stratospheric data before 1979 are considered unreliable, and we did not use the highly unusual winter-spring events of 2002, which included the only observed major stratospheric warming in the Southern Hemisphere.
 19. D. W. J. Thompson, J. M. Wallace, *J. Climate* **13**, 1000 (2000).
 20. The stratospheric NAM variance peaks in midwinter (6).
 21. W. A. Norton, *Geophys. Res. Lett.* **30**, 1627 (2003).
 22. The question of causality, i.e., whether the stratosphere causes changes to the troposphere, is irrelevant for the forecasting problem.
 23. A. J. Charlton, A. O'Neill, D. B. Stephenson, W. A. Lahoz, M. P. Baldwin, *Q. J. R. Meteorol. Soc.*, in press.
 24. We use the square of the anomaly correlation to measure skill.
 25. The AO accounts for 24% of the variance of monthly-mean 1000-hPa geopotential during December through February.
 26. Artificial skill is an overestimate of the real skill of a forecasting system caused by the inclusion of the same data to evaluate the skill that was used to develop or train the forecasting system. Artificial skill can be avoided by the use of independent training and assessment data sets. Artificial skill often occurs in practice because of the presence of long-term trends in the data set (42).
 27. Because it is persistent, the AO adds predictive skill on shorter time scales.
 28. MCA is also known as singular value decomposition analysis (41).
 29. T. G. Shepherd, *J. Meteorol. Soc. Japan* **80**, 769 (2002).
 30. V. Limpasuvan, D. H. Hartmann, *J. Climate* **13**, 4414 (2000).
 31. P. H. Haynes, T. G. Shepherd, *Q. J. R. Meteorol. Soc.* **115**, 1181 (1989).
 32. During December through February, the daily correlation between 300-hPa momentum-flux anomalies (latitudinally averaged north of 20°N) and the rate of change of the AO index is 0.46.
 33. D. Lorenz, D. Hartmann, *J. Climate*, **16**, 1212 (2003).
 34. They found similar lag correlations between the leading EOF of 1000- to 100-hPa zonal wind and eddy momentum-flux convergences.
 35. When the NAM strengthened with height, the mean was 0.028 and the standard deviation was 0.90. When the NAM weakened with height, the mean was -0.018 and the standard deviation was 1.06.
 36. P. Chen, W. A. Robinson, *J. Atmos. Sci.* **49**, 2533 (1992).
 37. P. H. Haynes, C. J. Marks, M. E. McIntyre, T. G. Shepherd, K. P. Shine, *J. Atmos. Sci.* **48**, 651 (1991).
 38. J. Perlwitz, H.-F. Graf, *Geophys. Res. Lett.* **28**, 271 (2001).
 39. J. Perlwitz, N. Harnik, *J. Climate*, in press.
 40. R. X. Black, *J. Climate*, **15**, 268 (2002).
 41. H. von Storch, F. W. Zwiers, *Statistical Analysis in Climate Research* (Cambridge Univ. Press, Cambridge, 1999), p. 321.
 42. I. T. Jolliffe, D. B. Stephenson, Eds. *Forecast Verification: A Practitioner's Guide in Atmospheric Science* (Wiley, New York, 2003), p. 203.
 43. We thank P. H. Haynes, D. A. Ortland, W. A. Robinson, S. Schubert, and T. G. Shepherd for discussions

and A. Worsham for assistance with Fig. 1C. Supported by NSF's Climate Dynamics Program, NOAA's Office of Global Programs, NASA's Supporting Research and Technology Program for Geospace Sciences, NASA's Living With a Star Program, and NASA's

Oceans, Ice, & Climate Program (M.P.B.); NSF's CAREER program (D.W.J.T.); and NOAA's Office of Global Programs (T.J.D.).

22 May 2003; accepted 3 July 2003

Role of Adaptor TRIF in the MyD88-Independent Toll-Like Receptor Signaling Pathway

Masahiro Yamamoto,¹ Shintaro Sato,^{1,2} Hiroaki Hemmi,¹ Katsuki Hoshino,^{1,4} Tsuneyasu Kaisho,^{1,4} Hideki Sanjo,¹ Osamu Takeuchi,¹ Masanaka Sugiyama,¹ Masaru Okabe,³ Kiyoshi Takeda,^{1,2} Shizuo Akira^{1,2*}

Stimulation of Toll-like receptors (TLRs) triggers activation of a common MyD88-dependent signaling pathway as well as a MyD88-independent pathway that is unique to TLR3 and TLR4 signaling pathways leading to interferon (IFN)- β production. Here we disrupted the gene encoding a Toll/IL-1 receptor (TIR) domain-containing adaptor, TRIF. TRIF-deficient mice were defective in both TLR3- and TLR4-mediated expression of IFN- β and activation of IRF-3. Furthermore, inflammatory cytokine production in response to the TLR4 ligand, but not to other TLR ligands, was severely impaired in TRIF-deficient macrophages. Mice deficient in both MyD88 and TRIF showed complete loss of nuclear factor kappa B activation in response to TLR4 stimulation. These findings demonstrate that TRIF is essential for TLR3- and TLR4-mediated signaling pathways facilitating mammalian antiviral host defense.

TLRs recognize specific patterns of microbial components and are critical in provoking innate immune responses through activation of signaling cascades via Toll/IL-1 receptor (TIR) domain-containing adaptors, such as MyD88 and TIRAP (1, 2). MyD88 is common to all the TLRs, whereas TIRAP is specifically involved in TLR2- and TLR4-mediated signaling pathways (3–5). In addition to the common MyD88-dependent pathway, TLR3 and TLR4 utilize a MyD88-independent signaling pathway that leads to the activation of IRF-3 and induction of IFN- β (6–8). TIR domain-containing adaptor inducing IFN- β (TRIF) was recently identified as a third adaptor and was shown to activate IFN- β expression via TLR3 (9, 10).

To assess the physiological role of TRIF, we generated mice lacking the *Trif* gene [supporting online material (SOM) Text and fig. S1]. Mutant mice homozygous for the disrupted *Trif* allele were born at the expected mendelian ratio and grew to be healthy in specific-pathogen-free conditions.

Previous in vitro studies have suggested that TRIF is involved in production of IFN- β in response to double-stranded RNA and its analog poly(I:C), both of which are recognized by TLR3 (9–11). Therefore, we first analyzed poly(I:C)-induced messenger RNA (mRNA) expression of IFN- β and several IFN-inducible genes, such as RANTES, IP-10, and MCP-1, in peritoneal macrophages (Fig. 1A). Macrophages from TRIF^{-/-} mice showed impaired expression of IFN- β and IFN-inducible genes in response to poly(I:C), which is consistent with results seen in TLR3^{-/-} mice (11, 12). In addition, splenocytes from TRIF^{-/-} mice showed severely defective proliferation in response to poly(I:C), but not to the TLR9 ligand CpG DNA (Fig. 1B). TRIF^{-/-} B cells were also severely impaired in poly(I:C)-induced, but not anti-IgM Ab (antibody to immunoglobulin M)-induced, augmentation of surface expression of CD69, CD86, and major histocompatibility complex (MHC) class II (Fig. 1C). Thus, TRIF^{-/-} mice showed defective responses to poly(I:C), indicating that TRIF is essential for TLR3-mediated signaling pathways.

In addition to the TLR3 ligand, the TLR4 ligand LPS has been shown to induce IFN- β and subsequent expression of IFN-inducible genes in a MyD88-independent manner (6–8). We analyzed LPS-induced mRNA expression of IFN-inducible genes

¹Department of Host Defense, Research Institute for Microbial Diseases, Osaka University, ²ERATO, Japan Science and Technology Corporation, ³Genome Information Research Center, 3-1 Yamada-oka, Suita Osaka 565-0871, Japan. ⁴RIKEN Research Center for Allergy and Immunology, 1-7-22 Suehiro-cho, Tsurumiku, Yokohama, Kanagawa 230-0045, Japan

*To whom correspondence should be addressed. E-mail: sakira@biken.osaka-u.ac.jp

such as RANTES, IP-10, and MCP-1 in embryonic fibroblast cells from TRIF-deficient mice (Fig. 2A). In TRIF^{-/-} cells, LPS-induced expression of IFN-inducible genes was severely reduced, demonstrating that TRIF^{-/-} mice were also defective in MyD88-independent responses to LPS.

We next analyzed inflammatory cytokine production in response to several TLR ligands, which is induced in a MyD88-dependent manner (Fig. 2B). Both wild-type and TRIF^{-/-} macrophages produced similar levels of interleukin-12 (IL-12) p40 in response to the TLR2 ligand peptidogly-

can, the TLR7 ligand R-848, and the TLR9 ligand CpG DNA (13, 14). However, LPS-induced production of tumor necrosis factor- α (TNF- α), IL-6, and IL-12 p40 was abolished in TRIF^{-/-} macrophages (Fig. 2, B and C). All wild-type animals injected with a lethal dose of LPS upon D-GalN (D-galactosamine hydrochloride) sensitization produced high concentrations of TNF- α and IL-6 and died within 24 hours of injection. (SOM Text and fig. S2). By contrast, TRIF^{-/-} mice showed defective production of inflammatory cytokines and resistance to LPS-induced septic shock. In addition, splenocytes from TRIF^{-/-} mice showed profoundly impaired proliferative responses to LPS, although these cells proliferated normally in response to R-848 (Fig. 2D) (13). Furthermore, LPS-induced augmentation of CD69 and CD86 expression was severely reduced in TRIF^{-/-} B cells, although anti-IgM Ab-induced expression was unaffected (Fig. 2E). Thus, TRIF^{-/-} mice showed defective responses to LPS in terms of both MyD88-dependent and MyD88-independent responses.

MyD88-independent signaling through TLR3 and TLR4 has been reported to activate the transcription factor IRF-3 (6, 8). Indeed, native-polyacrylamide gel electrophoresis (PAGE) analysis showed poly(I:C)- and LPS-induced formation of homophilic IRF-3 dimers in wild-type lung fibroblast cells and peritoneal macrophages, respectively (Fig. 3, A and B). How-

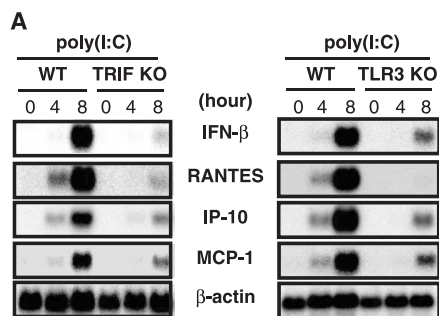
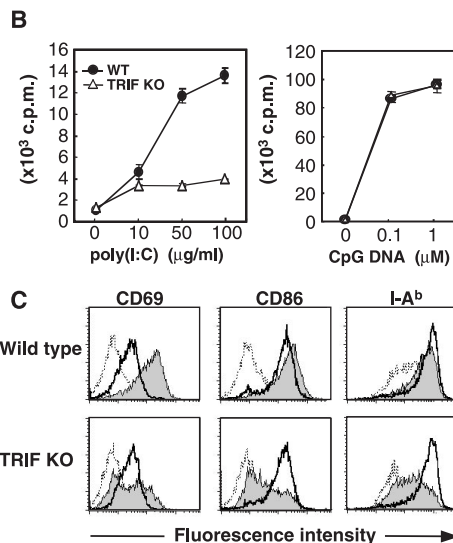
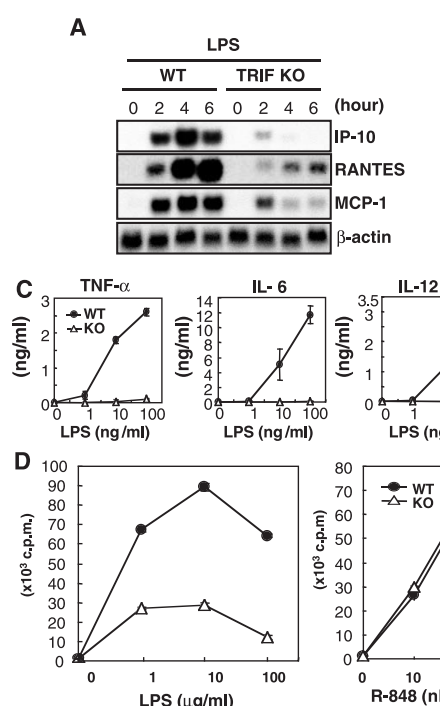


Fig. 1. Impaired responses to poly(I:C) in TRIF-deficient cells. (A) Peritoneal macrophages were stimulated with 50 μ g/ml poly(I:C) for the indicated periods. Total RNA (5 μ g) was extracted and subjected to Northern blot analysis for expression of IFN- β , IP-10, RANTES, and MCP-1. The same membrane was rehybridized with a β -actin probe. (B) Proliferation of poly(I:C)- or CpG DNA-stimulated splenocytes. Splenocytes were cultured with the indicated concentration of poly(I:C) or CpG DNA for 24 hours. [³H]-thymidine (1 μ Ci) was pulsed for the last 12 hours. [³H]-thymidine incorporation was measured by a scintillation counter. (C) Splenic B220⁺ cells were cultured with 50 μ g/ml poly(I:C) or 10 μ g/ml anti-IgM antibody. At the 36-hour culture period, cells were harvested and stained with biotin-conjugated antibodies to CD69 or CD86, or antibody to I-A^b followed by streptavidin-phycoerythrin (PE). Stained cells were analyzed on FACS Calibur using Cell Quest software. Area under dashed line represents cells cultured in medium; under solid line, α -IgM; shaded in gray, poly(I:C).

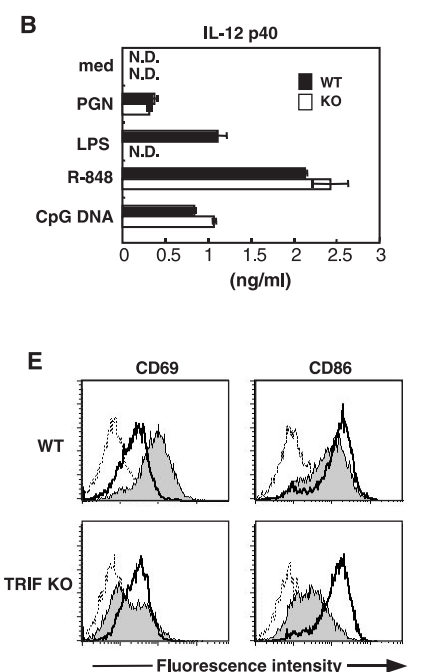


(B) Proliferation of poly(I:C)- or CpG DNA-stimulated splenocytes. Splenocytes were cultured with the indicated concentration of poly(I:C) or CpG DNA for 24 hours. [³H]-thymidine (1 μ Ci) was pulsed for the last 12 hours. [³H]-thymidine incorporation was measured by a scintillation counter. (C) Splenic B220⁺ cells were cultured with 50 μ g/ml poly(I:C) or 10 μ g/ml anti-IgM antibody. At the 36-hour culture period, cells were harvested and stained with biotin-conjugated antibodies to CD69 or CD86, or antibody to I-A^b followed by streptavidin-phycoerythrin (PE). Stained cells were analyzed on FACS Calibur using Cell Quest software. Area under dashed line represents cells cultured in medium; under solid line, α -IgM; shaded in gray, poly(I:C).

Fig. 2. Impaired responses to LPS in TRIF-deficient cells. (A) Embryonic fibroblasts were stimulated with 10 μ g/ml LPS for the indicated periods. Total RNA (10 μ g) was extracted and subjected to Northern blot analysis for expression of IP-10, RANTES, and MCP-1. The same membrane was rehybridized with a β -actin probe. (B) Peritoneal macrophages from TRIF-deficient mice or wild-type mice were left unstimulated or stimulated with 10 μ g/ml peptidoglycan (PGN), 100 ng/ml LPS, 100 nM R-848, or CpG DNA (1 μ M) in the presence of 30 ng/ml IFN- γ . Supernatants were collected for IL-12 p40 analysis by enzyme-linked immunosorbent assay (ELISA) 24 hours later. Indicated values are means \pm SD of triplicates. N.D., not detected. (C) Peritoneal macrophages were stimulated with the indicated concentrations of LPS in the presence of 30 ng/ml IFN- γ for 24 hours, and the supernatants were subjected to measurement of TNF- α , IL-6, and IL-12 p40 by ELISA. Indicated values are means \pm SD of triplicates. (D) Proliferation of LPS- or CpG DNA-stimulated splenocytes. Splenocytes were cultured with the indicated concentrations of LPS or CpG DNA for 24 hours. [³H]-thymidine (1 μ Ci) was pulsed for the last 12 hours. [³H]-thymidine incorporation was measured by a scintillation counter. (E) Splenic B220⁺ cells were cultured with 10 μ g/ml LPS or 10 μ g/ml anti-IgM antibody. At the 36-hour culture period, cells were harvested and stained with biotin-conjugated antibodies to CD69 or CD86 antibody followed by streptavidin-PE. Stained cells were analyzed on FACS Calibur using Cell Quest software. Areas under dashed and solid lines are as in Fig. 1C. Area under shaded line is for LPS.



(A) Embryonic fibroblasts were stimulated with 10 μ g/ml LPS for the indicated periods. Total RNA (10 μ g) was extracted and subjected to Northern blot analysis for expression of IP-10, RANTES, and MCP-1. The same membrane was rehybridized with a β -actin probe. (B) Peritoneal macrophages from TRIF-deficient mice or wild-type mice were left unstimulated or stimulated with 10 μ g/ml peptidoglycan (PGN), 100 ng/ml LPS, 100 nM R-848, or CpG DNA (1 μ M) in the presence of 30 ng/ml IFN- γ . Supernatants were collected for IL-12 p40 analysis by enzyme-linked immunosorbent assay (ELISA) 24 hours later. Indicated values are means \pm SD of triplicates. N.D., not detected. (C) Peritoneal macrophages were stimulated with the indicated concentrations of LPS in the presence of 30 ng/ml IFN- γ for 24 hours, and the supernatants were subjected to measurement of TNF- α , IL-6, and IL-12 p40 by ELISA. Indicated values are means \pm SD of triplicates. (D) Proliferation of LPS- or CpG DNA-stimulated splenocytes. Splenocytes were cultured with the indicated concentrations of LPS or CpG DNA for 24 hours. [³H]-thymidine (1 μ Ci) was pulsed for the last 12 hours. [³H]-thymidine incorporation was measured by a scintillation counter. (E) Splenic B220⁺ cells were cultured with 10 μ g/ml LPS or 10 μ g/ml anti-IgM antibody. At the 36-hour culture period, cells were harvested and stained with biotin-conjugated antibodies to CD69 or CD86 antibody followed by streptavidin-PE. Stained cells were analyzed on FACS Calibur using Cell Quest software. Areas under dashed and solid lines are as in Fig. 1C. Area under shaded line is for LPS.



REPORTS

ever, poly(I:C)- or LPS-induced dimerization of IRF-3 was not observed in TRIF^{-/-} cells. These findings demonstrate that TRIF is essential for MyD88-independent activation of IRF-3 in response to TLR3 and TLR4 signaling. In TLR3^{-/-} and TRIF^{-/-} cells, poly(I:C)-induced NF-κB activation was also severely impaired, indicating that TRIF plays a major role in TLR3-mediated NF-κB activation (Fig. 3C). In sharp contrast, LPS stimulation led to almost normal activation of NF-κB and mitogen-activated protein (MAP) kinase JNK in TRIF^{-/-} embryonic fibroblast cells (Fig. 3D). Moreover, LPS-induced autophosphorylation of IRAK-1, which is activated just downstream of MyD88, was intact in TRIF^{-/-} macrophages (SOM Text and fig. S3). In the case of TLR4 signaling, the MyD88-dependent pathway leads to an early-phase activation of NF-κB and MAP kinases, whereas the MyD88-independent pathway induces a late-phase activation of NF-κB and MAP kinases, as demonstrated by a delayed NF-κB and MAP kinase activation in MyD88^{-/-} cells (6, 15). Therefore, we hypothesized that the im-

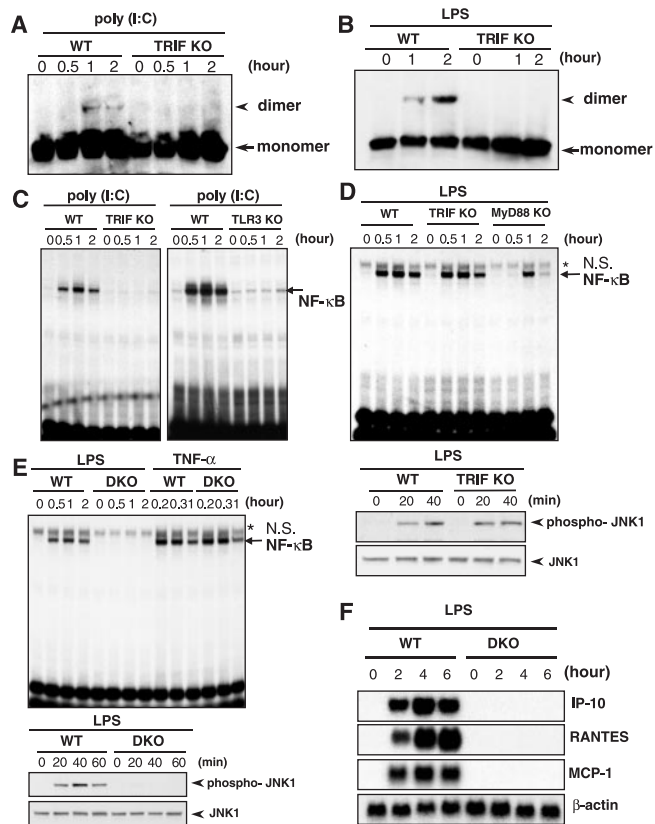
pairment in the TRIF-dependent late NF-κB and JNK activation was masked by the MyD88-dependent early activation in TRIF^{-/-} mice. To test this directly, we generated mice lacking both TRIF and MyD88. In embryonic fibroblast cells from TRIF/MyD88 double deficient mice, LPS-induced activation of NF-κB and JNK was completely inhibited (Fig. 3E). In addition, LPS induction of IFN-inducible genes such as IP-10, MCP-1, and RANTES was completely abolished in TRIF/MyD88 double-deficient cells (Fig. 3F). These findings clearly demonstrate that TRIF is essential for TLR4-mediated activation of the MyD88-independent signaling pathway.

We report the physiological function of TRIF revealed by analysis of TRIF^{-/-} mice, in which the MyD88-independent response induced by the TLR3 and TLR4 ligands was severely impaired. TRIF is an essential adaptor in TLR3 signaling because all the poly(I:C)-induced responses were abolished in TRIF^{-/-} mice. In the case of TLR4 stimulation, TRIF^{-/-} mice displayed normal

LPS-induced MyD88-dependent activation of IRAK-1, NF-κB, and MAP kinase, indicating that TRIF is not involved in the LPS-induced activation of the MyD88-dependent signaling. However, TRIF^{-/-} mice were impaired in the LPS-induced inflammatory cytokine production, which needs activation of the MyD88-dependent signaling. In this regard, we propose that cooperation of the MyD88-dependent and MyD88-independent (TRIF-dependent) signaling pathways are required for the TLR4-mediated inflammatory cytokine production. Recently, two noncanonical IκB kinases (IKKs), IKKε and TBK1, have been demonstrated to activate IRF-3 downstream of TRIF (16, 17). These IKKs have originally been shown to activate NF-κB (18–21). Therefore, IKKε and TBK1 are likely to have a role in TRIF-dependent activation of both NF-κB and IRF-3. Elucidation of physiologic roles for these IKKs in the TLR-mediated signaling pathways will clarify the precise mechanism by which the TRIF-dependent (MyD88-independent) signaling leads to activation of NF-κB and IRF-3.

In summary, we have identified an essential adaptor that regulates the MyD88-independent pathway, which is considered to be important in mediating antiviral host response. A precise analysis on the involvement of TRIF in the viral response of TRIF^{-/-} mice will provide a insight into the relation between TLRs and viral recognition.

Fig. 3. Activation of signaling cascade in TRIF-deficient and TRIF/MyD88 double-knockout cells. Lung fibroblasts (A) or peritoneal macrophages (B) were stimulated with (A) 50 μg/ml poly(I:C) or (B) 1 μg/ml LPS for the indicated periods. Cell lysates were prepared and subjected to native-PAGE. Monomeric (arrow) and dimeric (arrowhead) forms of IRF-3 were detected by Western blot. Lung fibroblasts were stimulated with (C) 50 μg/ml poly(I:C) and (D) 10 μg/ml LPS for the indicated periods. Nuclear extracts were prepared, and NF-κB DNA binding activity was determined by electrophoretic mobility shift assay (EMSA) using an NF-κB-specific probe. Arrows and asterisks indicate induced NF-κB complex and nonspecific bands (N.S.), respectively (upper panel). For the LPS-stimulated cells, JNK1 activation was also determined by western blotting using anti-phospho-JNK specific antibody toward the cell extracts (lower panel). (E) Embryonic fibroblasts from wild-type and TRIF/MyD88 double-deficient (DKO) mice were stimulated with 10 μg/ml LPS or 10 ng/ml TNF-α for the indicated periods. Nuclear extracts were prepared and NF-κB DNA binding activity was determined by EMSA using an NF-κB-specific probe. Arrows and asterisks indicate induced NF-κB complex and nonspecific bands, respectively (upper panel). For the LPS-stimulated cells, JNK1 activation was also determined by western blotting using anti-phospho-JNK specific antibody toward the cell extracts (lower panel). (F) Embryonic fibroblasts from wild-type and TRIF/MyD88 DKO mice were stimulated with 10 μg/ml LPS for the indicated periods. Total RNA (10 μg) was extracted and subjected to Northern blot analysis for expression of IP-10, RANTES, and MCP-1. The same membrane was rehybridized with a β-actin probe.



References and Notes

1. C. A. Janeway Jr., R. Medzhitov, *Annu. Rev. Immunol.* **20**, 197 (2002).
2. K. Takeda, T. Kaisho, S. Akira, *Annu. Rev. Immunol.* **21**, 335 (2003).
3. S. Akira, T. Kaisho, T. K. Takeda, *Nature Immunol.* **2**, 675 (2001).
4. M. Yamamoto et al., *Nature* **420**, 324 (2002).
5. T. Horng, G. M. Barton, R. A. Flavell, R. Medzhitov, *Nature* **420**, 329 (2002).
6. T. Kawai et al., *J. Immunol.* **167**, 5887 (2001).
7. K. Hoshino, T. Kaisho, T. Iwabe, O. Takeuchi, S. Akira, *Int. Immunol.* **14**, 1225 (2002).
8. S. Doyle et al., *Immunity* **17**, 251 (2002).
9. M. Yamamoto et al., *J. Immunol.* **169**, 6668 (2002).
10. H. Oshiumi, M. Matsumoto, K. Funami, T. Akazawa, T. Seya, *Nature Immunol.* **4**, 161 (2003).
11. L. Alexopoulou, A. C. Holt, R. Medzhitov, R. A. Flavell, *Nature* **413**, 732 (2001).
12. O. Takeuchi, S. Akira, unpublished data.
13. H. Hemmi et al., *Nature Immunol.* **3**, 196 (2002).
14. H. Hemmi et al., *Nature* **408**, 740 (2000).
15. T. Kawai, O. Adachi, T. Ogawa, K. Takeda, S. Akira, *Immunity* **11**, 115 (1999).
16. K. A. Fitzgerald et al., *Nature Immunol.* **4**, 491 (2003).
17. S. Sharma et al., *Science* **300**, 1148 (2003).
18. T. Shimada et al., *Int. Immunol.* **11**, 1357 (1999).
19. J. L. Pomerantz, D. Baltimore, *EMBO J.* **18**, 6694 (1999).
20. R. T. Peters, S. M. Liao, T. Maniatis, *Mol. Cell* **5**, 513 (2000).
21. F. Nomura, T. Kawai, K. Nakanishi, S. Akira, *Genes Cells* **5**, 191 (2000).
22. We thank H. Tomizawa for kindly providing R-848. We also thank T. Kawai, S. Uematsu, and H. Kuwata for helpful discussions; M. Hashimoto for secretarial assistance; and N. Okita and N. Iwami for technical

assistance. Supported by grants from Special Coordination Funds; the Ministry of Education, Culture, Sports, Science and Technology; Research Fellowships of the Japan Society for the Promotion of Science for Young Scientists; The Uehara Memorial Foundation; and The Naito Foundation.

Supporting Online Material
www.sciencemag.org/cgi/content/full/1087262/DC1
Materials and Methods
SOM Text
Figs. S1 to S3

References

27 May 2003; accepted 27 June 2003
Published online 10 July 2003;
10.1126/science.1087262
Include this information when citing this paper.

Evidence for Selective Advantage of Pathogenic FGFR2 Mutations in the Male Germ Line

Anne Goriely,¹ Gilean A. T. McVean,³ Maria Røjmyr,⁴ Björn Ingemarsson,⁴ Andrew O. M. Wilkie^{1,2*}

Observed mutation rates in humans appear higher in male than female gametes and often increase with paternal age. This bias, usually attributed to the accumulation of replication errors or inefficient repair processes, has been difficult to study directly. Here, we describe a sensitive method to quantify substitutions at nucleotide 755 of the fibroblast growth factor receptor 2 (*FGFR2*) gene in sperm. Although substitution levels increase with age, we show that even high levels originate from infrequent mutational events. We propose that these *FGFR2* mutations, although harmful to embryonic development, are paradoxically enriched because they confer a selective advantage to the spermatogonial cells in which they arise.

Striking male biases in mutation rate are observed in many human genetic disorders. Among these, three genes (*RET*, *FGFR2*, and *FGFR3*) encoding receptor tyrosine kinase proteins stand out because of the very high apparent rate of specific nucleotide substitutions and near-exclusive paternal origin of mutations (1, 2). We focused this work on position 755 of *FGFR2* (normally a cytosine, 755C), which shows the highest inferred mutation rate within this gene (3).

The local sequence context of the 755C nucleotide, part of a CpG doublet, is shown in Fig. 1A. Heterozygous 755 C-to-G (C>G) transversions (4) cause ~66% of cases of Apert syndrome (5, 6), a dominantly inherited malformation (7) that usually occurs by new mutation. The mutations arise exclusively from the unaffected father and are associated with increased paternal age (8, 9). On the basis of the observed birth prevalence of Apert syndrome of ~1 in 70,000 (10, 11), the apparent rate of 755C>G mutations in sperm is 9.4×10^{-6} , which is elevated 200- to 800-fold over the background genomic rate for C>G transversions at CpG dinucleotides (12, 13). Of the other possible heterozygous substitutions at position 755, C>A has not

been documented, but the C>T transition was identified in five subjects from two families and was associated with a normal or mild Crouzon syndrome phenotype (7, 14, 15). Highlighting the unusual mutability of the 755C nucleotide, the C>T has also been described in cis with four additional mutations, generating the mutant *FGFR2* alleles 755_756CG>TT (14, 16), 755_756CG>TC (15), 755_757CGC>TCT (14) (Fig. 1A), and 755C>T; 943G>T (17). In the heterozygous state, these multiple mutations (expected to occur at rates of $\sim 10^{-11}$) (13) are consistently associated with more severe phenotypes (Apert syndrome, Pfeiffer syndrome, or severe syndactyly) (7) than 755C>T alone.

We developed a protocol to enrich samples for mutations at 755C (Fig. 1B). Genomic DNA samples were digested with *MboI*, which cuts only the normal sequence (Fig. 1A); the undigested fraction was amplified by polymerase chain reaction (PCR), further enriched by repeat *MboI* digestion, and quantified with the use of Pyrosequencing technology (Pyrosequencing AB, Uppsala, Sweden) and statistical modeling (18) (fig. S1A). To determine absolute mutation levels, samples were spiked with two concentrations of genomic DNA from the patient ("GR") heterozygous for the 755_757CGC>TCT substitution. Representative pyrograms are shown in Fig. 1, C and D.

To validate the method, we quantified the 755C>G mutation when progressively diluted with normal DNA from blood (Fig. 2A). At mutant concentrations of $\geq 10^{-5}$ (comparable to the birth rate of Apert syndrome),

point estimates were accurate within twofold; below 10^{-5} , mutation levels were overestimated, probably because of in vitro DNA damage and PCR errors (19). Next, we undertook pilot analyses of sperm samples from an individual with a relatively high 755C>G count (Fig. 2B). We obtained consistent estimates both in sample replicates and in different samples, indicating that analysis of single sperm samples accurately reflects mutation prevalence in the individual (18) (fig. S2A).

We next measured mutation levels in samples from three sources: (i) blood from healthy individuals ($n = 11$), (ii) sperm from healthy men without a family history of Apert syndrome ($n = 99$), and (iii) sperm from unaffected fathers of children with Apert syndrome caused by the 755C>G mutation ($n = 6$). The levels of 755 C>G, C>T, and C>A are shown in Fig. 3A, B, and C, respectively. Only low levels ($< 10^{-5}$) of all mutations were found in blood, which excludes the possibility that higher levels in sperm were caused by contamination or PCR artifacts. In sperm, the level of 755C>A never exceeded 6.3×10^{-6} and showed no paternal age effect ($r = -0.06$, $P = 0.71$), but both 755C>G and 755C>T reached high levels (maxima of 1.6×10^{-4} and 1.4×10^{-4} , respectively), that were positively correlated with donor age ($r = 0.39$, $P < 0.0001$ for 755C>G; $r = 0.45$, $P < 0.0001$ for 755C>T). The average level of 755C>G was 1.66-fold higher than that of 755C>T (permutation test, $P < 0.05$). Levels of the 755C>G mutation in the sperm of fathers of Apert syndrome children all fell within the envelope of normal values (Fig. 3A), indicating that these men are sampled from the general population and have a very low risk of fathering another affected child.

One sperm sample from a normal 37-year old donor showed an atypical pyrogram with different heights of the two peaks diagnostic for 755T (Fig. 1E); this would occur if an additional substitution at 756G had occurred (fig. S1A). We cloned and sequenced the *MboI*-digested PCR product from this individual and demonstrated that ~20% of 755T sequences harbored the double mutation 755_756CG>TC (Fig. 1F), which causes Apert syndrome (14–16).

We compared our measurements of sperm mutation prevalence in the population with paternal age data for a cohort of Apert patients (18). The increase in levels of the 755C>G mutation in sperm with donor age

¹Weatherall Institute of Molecular Medicine, ²Nuffield Department of Clinical Laboratory Sciences, John Radcliffe Hospital, University of Oxford, Oxford OX3 9DS, UK. ³Department of Statistics, University of Oxford, South Parks Road, Oxford OX1 3TG, UK. ⁴Pyrosequencing AB, Vallongatan 1, SE-752 28 Uppsala, Sweden.

*To whom correspondence should be addressed. E-mail: awilkie@hammer.imm.ox.ac.uk